Supplementary Information for:

Millisecond Coherence Time in a Tunable Molecular Electronic Spin Qubit

Joseph M. Zadrozny,[1] Jens Niklas,[2] Oleg G. Poluektov,[2] and Danna E. Freedman[1]*

[1] *Department of Chemistry, Northwestern University, Evanston, Illinois 60208*

[2] *Chemical Sciences and Engineering Division, Argonne National Laboratory, Argonne, Illinois 60439, USA.*

Table of Contents

Full Experimental Details.

General Considerations. 4,5-Dibenzoyl-1,3-dithiole-1-thione $(PhCO)_2(\alpha\text{-}C_3S_5)$,[1] 4,5-dimercapto-1,2-dithiole-3-thione $(PhCO)_2(\beta\text{-}C_3S_5)$,[2] $VCl_3(THF)_3$,[3] (d^{20}-Ph_4P)Br,[4] thiapendione ($C_2O_2S_2$),[5] and $(Ph_4P)_2[V(C_8S_8)_3]$ (**1**)[6] were prepared according to literature procedures. Diethylether (Et_2O), tetrahydrofuran (THF), dimethylformamide (DMF), methanol (MeOH), carbon disulfide (CS_2) and acetonitrile (MeCN) were dried according to published procedures and degassed by three consecutive freeze-pump-thaw cycles or Ar sparging prior to use.[7] Deuterated DMF and toluene were degassed by three consecutive freeze pump thaw cycles and dried either over activated sieves (d^7-DMF) or NaK alloy (d^8-tol) prior to use. All other reagents were employed as received.

(d^{20}-Ph_4P)$_2$[V(C_8S_8)$_3$] (1′) This complex was prepared following the same procedure as $(Ph_4P)_2[V(C_8S_8)_3]$ utilizing the deuterated salt (d^{20}-Ph_4P)Br. IR (cm^{-1}): 2919(w), 2855(w), 1545(m), 1488(m), 1431(m), 1406(w), 1382(m), 1329(w), 1297(s), 1265(m), 1166(m), 1092(m), 1050(vs), 951(s), 898(w), 862(s), 834(s), 693(m), 658(m), 541(s), 495(vs), and 445(s) cm^{-1}. ESI/MS (*m*/*z*): $\{V(C_8S_8)_3\}^{2-}$, 554.03 (base); $\{(d^{20}\text{-}Ph_4P)[V(C_8S_8)_3]\}^{-}$, 1467.47; $\{[V(C_8S_8)_2]\}^{-}$, 754.38.

$(Ph_4P)_2[V(\beta\text{-}C_3S_5)_3]$ (2) Under an inert atmosphere, a solution of NaOMe (121 mg, 2.24 mmol) in 5 mL of MeOH was added to a stirring slurry of $(PhCO)_2[\beta\text{-}C_3S_5]$ (454 mg, 1.12 mmol) in 5 mL of MeOH. The solution was allowed to stir until a clear dark orange solution was obtained. To this solution, $VCl_3(THF)_3$ (138 mg, 0.369 mmol) in 3 mL of MeOH was added dropwise with stirring, yielding a dark brownish red solution. After stirring for 10 m, a solution of $(Ph_4P)Br$ (310 mg, 0.739 mmol) in 5 mL of MeOH was added to the solution dropwise, yielding a dark red precipitate. The reaction mixture was stirred for an additional half hour, then exposed to air, and allowed to stir an additional half hour. The black precipitate was filtered and washed with 5 mL of MeOH followed by 5 mL of Et_2O in air. This solid was then redissolved in 20 mL of DMF and layered under 100 mL MeOH, to provide X-ray quality crystals of the title compound (100 mg, 21%). IR (cm^{-1}): 3050(w), 1584(m), 1480(m), 1432(s), 1353(s), 1253(vs), 1228(w), 1186(w), 1159(w), 1102(s), 1049(s), 982(s), 929(s), 818(s), 745(w), 718(s), 684(s), and 520(vs).

ESI/MS (*m*/*z*): $\{V(C_3S_5)_3\}^{2-}$, 319.26 (base); $\{(Ph_4P)[V(C_3S_5)_3]\}^-$, 977.60; $\{[V(C_3S_5)_2]\}^-$, 442.58. Anal. Calcd. for $C_{57}H_{40}P_2VS_{15}$: 51.91 %C; 3.06 %H. Found: 51.73 %C; 3.01 %H.

$(Ph_4P)_2[V(\alpha\text{-}C_3S_5)_3]$ (3) $(PhCO)_2(\alpha\text{-}C_3S_5)$ (327 mg, 0.804 mmol) and NaOMe (82 mg, 1.5 mmol) were combined in 10 mL of THF and stirred vigorously for 0.5 hr. The solution was evaporated to dryness *in vacuo* and titurated with 20 mL of Et_2O, leaving a red powder and yellow solution. The yellow solution was decanted from the powder and the process repeated, followed by drying of the powder *in vacuo* for 1 hr. The powder was redissolved in 10 mL of THF to produce a red solution, to which was added a solution of $VCl_3(THF)_3$ (94 mg, 0.25 mmol) in 5 mL of THF with vigorous stirring. The resultant brown/red solution was exposed to air and stirred for a half hour. To this solution was added a 3 mL solution of $(Ph_4P)Br$ in MeCN (204 mg, 0.486 mmol), which was then allowed to stir for 5 m. Et_2O was added to precipitate a crude brown solid, which was recrystallized by diffusion of Et_2O vapor into an acetone solution to give dark red needles (185 mg, 57 %) of the title compound. IR (cm^{-1}): 3050(w), 1707(m), 1583(m), 1481(m), 1435(s), 1392(m), 1357(w) 1336(w), 1311(w), 1216(w), 1184(w), 1163(w), 1106(vs), 1046(vs), 1025(s), 993(s), 890(m), 848(m), 749(s), 718(vs), 687(vs), 523(vs), 467(s), and 445(m). ESI/MS (*m*/*z*): $\{V(C_3S_5)_3\}^{2-}$, 319.225 (base); $\{(Ph_4P)[V(C_3S_5)_3]\}^-$, 977.67; $\{[V(C_3S_5)_2]\}^-$, 442.6; $\{V(C_3S_5)_3\}^-$, 628.511. Anal. Calcd. for $C_{57}H_{40}P_2S_{15}V$: 51.91 %C; 3.05 %H. Found: 51.48 %C; 3.08 %H.

$(Ph_4P)_2[V(C_3S_4O)_3]$ (4) Solid NaOMe (89 mg, 1.6 mmol) and thiapendione (171 mg, 0.82 mmol) were reacted in 5 mL of MeOH in an aluminum foil-wrapped vial to yield a yellow solution. To this solution $VCl_3(THF)_3$ (101 mg, 0.270 mmol) dissolved in 5 mL of MeOH was added generating a dark green solution. A solution of $(Ph_4P)Br$ (201 mg, 0.479 mmol) in 5 mL of MeOH was added and a green precipitate formed. The reaction mixture was filtered and stored at –35 °C to yield a dark green crystalline solid (120 mg, 50%). Single crystals of sufficient quality for X-ray diffraction were prepared by diffusion of Et_2O vapor into a mother liquor of MeCN. IR (cm^{-1}): 3053(m), 1657(vs), 1604(vs), 1481(s), 1435(vs), 1339(w), 1311(w), 1188(m), 1163(m), 1106(vs), 1028(m), 997(s), 968(w), 887(m), 749(s), 721(vs), 685(vs), 523(vs), and 467(s). ESI/MS (*m*/*z*): $\{V(C_3S_4O)_3\}^{2-}$, 295.31 (base); $\{(Ph_4P)[V(C_3S_4O)_3]\}^-$, 929.68;

{[V($C_3S_4O)_2$]}$^-$, 410.63. Anal. Calcd. for $C_{57}H_{40}O_3P_2S_{12}V$: 53.88 %C; 3.17 %H. Found: 53.60 %C; 3.16 %H.

X-ray Data Collection, Structure Solution and Refinement for 2-4. Data for **2-4** were collected at the X-ray Crystallography lab of the Integrated Molecular Structure Education and Research Center of Northwestern University. Data collections for **2-4** were performed on single crystals coated in Paratone-N oil and mounted on MicroMounts^{TM} rods under freezing streams of N_2. During mounting, crystals of **2-4** did not show any signs of desolvation or other decomposition. Data were collected for **3** and **4** using a Bruker KAPPA diffractometer equipped with a Cu Kα (λ = 1.54178 Å) Iμs microfocus X-ray source with MS Optics, an APEX-II detector, and Oxford Cryosystems Cryostream cryostat. Data for **2** were collected on a Bruker KAPPA diffractometer with a Cu Kα (λ = 1.54178 Å) Iμs microfocus source with Quazar Optics, and APEX-II detector, and Oxford Cryosystems Cryostream cryostat. Raw data were integrated and corrected for Lorentz and polarization effects using Bruker Apex2 v. 2013.2.[8] Absorption corrections were applied using SADABS.[9] The space group was determined by examination of systematic absences, *E*-statistics, and successive refinement of the structure. The crystal structure was solved with direct methods and further refined with SHELXL[10] operated with the OLEX2 interface.[11] The crystal did not show significant decay during data collection. Thermal parameters were refined anisotropically for all non-hydrogen atoms or ions in **2-4** except for light atoms modeled as disordered. Disordered solvent molecules, where present, were modeled with the use of free variables. Hydrogen atoms were placed in ideal positions and refined using a riding model for all structures. Full crystal tables for **2-4** are provided in Tables S1-S4.

Electron Paramagnetic Resonance. Samples of **1**-**4** were dissolved in the respective solvents under an inert atmosphere, frozen in a 4 mm OD Wilmad quartz tube, and flame sealed under vacuum. CW and pulsed EPR measurements were performed at X-band frequency (~9.8 GHz) with a Bruker ELEXSYS E580 EPR spectrometer (Bruker Biospin, Rheinstetten, Germany), equipped with a 1 kW TWT amplifier (Applied Systems Engineering, Fort Worth) and helium cryostat gas-flow cryostat (CF935, Oxford Instruments, UK). The temperature was controlled by an ITC (Oxford, Instruments, UK). A Flexline dielectric ring ENDOR resonator (Bruker EN

4118X-MD4-W1) was used. Field-swept electron spin echo-detected EPR spectra were recorded using a two-pulse echo sequence with microwave (mw) pulses of 32 and 48 ns and an interpulse time of 140 ns for all species except **1′** in CS_2, which used a 160 ns interpulse delay. Echo decay curves were collected by application of the above sequence at the central resonance of each solution with increasing τ. T_2 at 10 K did not vary from 1 to 0.05 mM concentrations for **1** in PrCN, suggesting that intermolecular contributions to decoherence are not significant at the measured concentrations of this report. Inversion recovery curves were collected via application of a three-pulse ($\pi - \pi/2 - \pi$) inversion recovery sequence with (52 – 32 - 48) ns pulse lengths for all samples except **1′** which was (36 – 16 - 32). Data were manipulated in Origin 9.0.[12] All inversion recovery data were better fit by biexponential functions with long and short T_1 values than monoexponential recoveries. Addition of further exponential recovery terms insignificantly improved the fits. We note that the occurrence of a distribution of relaxation times in a spin system frequently yields recovery curves that are better modeled by biexponential curves than monoexponential curves (ref 18 of main report). Importantly, the temperature dependences of T_1 values are nearly the same across **1-4** in a given solvent system regardless of whether a mono or biexponential fit was used. Here, we used the slow T_1 for all complexes for consistency during comparisons from **1-4**. Spin-spin relaxation times (T_2) were determined generally by fitting the decay of the echo intensity to stretched exponential functions with exponents x close to 1. Instances where biexponential fits were used include **1′** in CS_2 and DMF/Tol samples of **1**-**4**. We note that the presence of the fast relaxation at low 2τ may be, in the case of CS_2, precipitation/crystallization of a small fraction of the sample with short intermolecular contacts owing to the fact that CS_2 does not glass when frozen. In the case of DMF/Tol, the fast relaxation process may be due to rotating methyl groups, as evidenced by its disappearance in the results for the d_7-DMF/d_8-Tol solvent system. The ratio of pre-exponential factors for fast to slow relaxation terms in biexponential fits were generally 0.3 or lower. Where ESEEM was present, only the data points at the top of the oscillations were used for fitting. For two solvent systems, DMF/Tol and CS_2, a biexponential function was used owing to a fast relaxation regime at short 2τ values. Nutation data were normalized and zero filled by 1024 points prior to performing the Fourier transform with a Hamming window. Peaks in the FT of the nutation data at 14.7 MHz arise from protons in the solvents.[13]

Continuous wave spectra were fit using Easyspin.[14] The model employed an $S = {}^1/_2$ electronic spin coupled to an $I = {}^7/_2$ nuclear spin (expected for a ^{51}V nucleus) and generates an eight-line pattern in both continuous wave and pulsed X-band EPR spectra (see Figs. S1). This coupling is well described by the model spin Hamiltonian:

$$\hat{H} = g\mu_B \boldsymbol{HS} + \boldsymbol{IAS} \qquad (1)$$

where g is the g-tensor, μ_B the Bohr magneton, $\boldsymbol{H}$ the magnetic field, $\boldsymbol{S}$ electronic spin, $\boldsymbol{I}$ the nuclear spin of the ^{51}V nucleus, and $\boldsymbol{A}$ the hyperfine coupling interaction tensor. The first term describes the interaction of the electronic spin with the applied magnetic field and the second describes the hyperfine coupling. Our prior analysis of $[V(C_8S_8)_3]^{2-}$ revealed axial g- and A-tensors, where $g_z = 1.992$, $g_x = g_y = 1.972$, $A_x = A_y = -258$ MHz. $A_z = 6$ MHz (ref 12 in main text). Here, we note that this model assigns the EPR transitions to that spanning from $|-{}^1/_2, +{}^7/_2\rangle \rightarrow |+{}^1/_2, +{}^7/_2\rangle$ at low field to $|-{}^1/_2, -{}^7/_2\rangle \rightarrow |+{}^1/_2, -{}^7/_2\rangle$ at high field for all species. The, strongest, sharpest transition observed both in the cw and pulsed EPR spectra is the transition $|-{}^1/_2, +{}^1/_2\rangle \rightarrow |-{}^1/_2, +{}^1/_2\rangle$. All pulsed studies reported here focus on this sharp central resonance. Fits to data for **1-4** in 1:1 DMF/Tol, depicted in Figure S8, proceeded analogously, yielding the parameters tabulated in Table S5. The relative magnitudes of $A_{x,y}$ to A_z here indicate that the unpaired electron is in the d_{z2} orbital of the V(IV) ion in accord with prior investigations of the V(IV) trisdithiolate class of compounds.[15-18]

Other Physical Measurements. Combustion analyses were performed by Midwest Microlab (Indianapolis, IN). Infrared spectra were recorded on a Bruker Alpha FTIR spectrometer equipped with an attenuated total reflectance accessory. Electrospray ionization mass spectrometry measurements were performed on acetonitrile solutions of **1**-**4** with a Bruker Amazon X ESI-Ion Trap Mass Spectrometer at the IMSERC facility of Northwestern. Cyclic voltammetry measurements were carried out in a standard one-compartment cell under nitrogen, equipped with platinum working and counter electrodes, a silver wire reference electrode and a CHI 760c potentiostat. Analyte solutions were prepared with 0.1 mM tetrabutylammonium hexafluorophosphate in MeCN. Ferrocene was used as an internal standard and all potentials are referenced to the $[Cp_2Fe]^{0/1+}$ couple.

Table S1 | Crystallographic information for the structural refinement of **2**.

Empirical Formula	$C_{57}H_{40}P_2S_{15}V$
Formula weight	1318.67 g/mol
Temperature	100(2) K
Radiation	CuKα (λ = 1.54178 Å)
Crystal System	Monoclinic
Space Group	*C* 2/c
Unit Cell Dimensions	a = 22.9413(7) Å, α = 90°
	b = 15.3812(5) Å, β = 78.6184(8)°
	c = 17.2844(5) Å, γ = 90°
Volume	5680.4(3) Å^3
Z	4
Density (calculated)	1.542 Mg/m^3
Absorption coefficient	7.461 mm^{-1}
F_{000}	2700
Crystal color	Dark brown
Crystal size	0.101 × 0.053 × 0.046 mm^3
2θ range	7.082 to 130.272°
Index ranges	$-23 \le h \le 26$
	$-18 \le k \le 16$
	$-20 \le l \le 20$
Reflections collected	23582
Independent reflections	4853[R_{int} = 0.0244]
Completeness to θ = 26.00°	99.8 %
Absorption correction	Multi-scan
Maximum and minimum transmission	0.753 and 0.586
Refinement method	Full-matrix least-squares on F^2
Data / restraints / parameters	4853 / 30 / 351
Goodness-of-fit on F^{2a}	1.197
Final *R* indices [I > 2σ(I) = 4853 data]^b	R_1 = 2.98 %, wR_2 = 6.96 %
R indices (all data, 0.80 Å)	R_1 = 3.00 %, wR_2 = 6.96 %
Largest diff. peak and hole	0.53 and –0.26 e.Å^{-3}

^{a} GooF = $[\Sigma[w(F_o^2-F_c^2)^2] / (n-p)]^{1/2}$ where n is the number of reflections and p is the total number of parameters refined. $^b R_1 = \Sigma||F_o|-|F_c|| / \Sigma|F_o|$; $wR_2 = [\Sigma[w(F_o^2-F_c^2)^2] / \Sigma[w(F_o^2)^2]\ ]^{1/2}$

Table S2 | Crystallographic information for the structural refinement of **3**.

Empirical Formula	$C_{60}H_{46}OP_2S_{15}V$
Formula weight	1376.75 g/mol
Temperature	100(2) K
Radiation	CuKα (λ = 1.54178 Å)
Crystal System	Triclinic
Space Group	*P*–1
Unit Cell Dimensions	a = 11.0006(6) Å, α = 88.133(3)°
	b = 14.0913(8) Å, β = 83.986(3)°
	c = 20.2928(11) Å, γ = 78.554(3)°
Volume	3065.9(3) Å^3
Z	2
Density (calculated)	1.491 Mg/m^3
Absorption coefficient	6.950 mm^{-1}
F_{000}	1414.0
Crystal color	Red
Crystal size	0.254 × 0.091 × 0.063 mm^3
2θ range	4.378 to 133.222°
Index ranges	$-13 \le h \le 7$
	$-16 \le k \le 16$
	$-22 \le l \le 23$
Reflections collected	23018
Independent reflections	10255 [R_{int} = 0.0301]
Completeness to 2θ = 133.222°	94.7 %
Absorption correction	Multi-scan
Maximum and minimum transmission	0.754 and 0.600
Refinement method	Full-matrix least-squares on F^2
Data / restraints / parameters	10255 / 0 / 714
Goodness-of-fit on F^{2a}	1.088
Final *R* indices [I > 2σ(I) = 10255 data]^b	R_1 = 3.45 %, wR_2 = 8.45 %
R indices (all data, 0.80 Å)	R_1 = 4.02 %, wR_2 = 8.68 %
Largest diff. peak and hole	0.48 and –0.37 e.Å^{-3}

^{a} GooF = $[\Sigma[w(F_o^2-F_c^2)^2] / (n-p)]^{1/2}$ where n is the number of reflections and p is the total number of parameters refined. $^b R_1 = \Sigma||F_o|-|F_c|| / \Sigma|F_o|$; $wR_2 = [\Sigma[w(F_o^2-F_c^2)^2] / \Sigma[w(F_o^2)^2]\ ]^{1/2}$

Table S3 | Crystallographic information for the structural refinement of **4**.

Empirical Formula	$C_{58}H_{44}O_4P_2S_{12}V$
Formula weight	1302.8 g/mol
Temperature	100(2) K
Radiation	CuKα (λ = 1.54178 Å)
Crystal System	Triclinic
Space Group	*P*–1
Unit Cell Dimensions	a = 10.6733(7) Å, α = 96.429(2)°
	b = 13.8411(9) Å, β = 90.582(2)°
	c = 21.2149(14) Å, γ = 110.889(2)°
Volume	2905.4(3) Å^3
Z	2
Density (calculated)	1.489 Mg/m^3
Absorption coefficient	6.358 mm^{-1}
F_{000}	1337.9
Crystal color	Greenish blue
Crystal size	0.164 × 0.133 × 0.086 mm^3
2θ range	7.612 to 133.236°
Index ranges	$-12 \le h \le 10$
	$-12 \le k \le 16$
	$-25 \le l \le 23$
Reflections collected	24008
Independent reflections	10028 [R_{int} = 0.0422]
Completeness to 2θ = 133.222°	97.6 %
Absorption correction	Multi-scan
Maximum and minimum transmission	0.753 and 0.588
Refinement method	Full-matrix least-squares on F^2
Data / restraints / parameters	10028 / 118 / 728
Goodness-of-fit on F^{2a}	1.060
Final *R* indices [I > 2σ(I) = 10255 data]^b	R_1 = 4.71 %, wR_2 = 12.02 %
R indices (all data, 0.80 Å)	R_1 = 5.70 %, wR_2 = 12.66 %
Largest diff. peak and hole	0.85 and –0.47 e.Å^{-3}

^{a} GooF = $[\Sigma[w(F_o^2-F_c^2)^2] / (n-p)]^{1/2}$ where n is the number of reflections and p is the total number of parameters refined. $^b R_1 = \Sigma||F_o|-|F_c|| / \Sigma|F_o|$; $wR_2 = [\Sigma[w(F_o^2-F_c^2)^2] / \Sigma[w(F_o^2)^2]\ ]^{1/2}$

Table S4. Select mean interatomic parameters for **1**-**4**.

	1[a]	**2**	**3**	**4**
V–S (Å)	2.37(2)	2.37(4)	2.38(1)	2.39(1)
S–V–S (°)[b]	84(1)	84.8(7)	85(1)	84.9(4)
S–C (Å)[c]	1.740(5)	1.72(2)	1.729(3)	1.739(7)
C–C (Å)[d]	1.401(4)	1.369(3)	1.356(1)	1.36(2)
V•••V(Å)[e]	10.70(1)	10.82(1)	10.51(1)	10.81(1)

[a]Data from ref 12. [b]Ligand bite angles. [c]S–C distances for the sulfur atoms bound directly to the V(IV) ion. [d]For the C=C double bond that bridges the two thiolate donor atoms.[e]Nearest interionic distance.

Table S5. Summary of spin Hamiltonian parameters for **1**-**4** determined by simulating cw EPR spectra.[a]

	1	**2**	**3**	**4**
g_x[b]	1.968	1.969[f]	1.956	1.959	1.960
g_y[b]	1.970	1.971[f]	1.954	1.958	1.964
g_z[b]	1.990	1.990[f]	1.986	1.980	1.981
A_x[c]	–261	–265[f]	–342	–348	–319
A_y[c]	–269	–274[f]	–338	–310	–341
A_z[c,d]	46	45[f]	65	46	57
$\langle A \rangle$[e]	–170	–165[f]	–205	–204	–201

[a]All spectra were collected at 40 K in 1:1 DMF/PrCN, except for **1**, which was collected in both 1:1 DMF/PrCN and pure PrCN. [b]Estimated errors for these parameters are ±0.002. [c]Estimated errors are: $A_{x,y}$, ± 5 and A_z, ±10 MHz. [d]The sign of A_z is ill-defined in these experiments; designated negative because of presumed dominance of Fermi-contact contribution to A. See refs 15-18. [e]$\langle A \rangle = (A_x + A_y + A_z)/3$. [f]From spectrum obtained in pure PrCN.

Table S6. Tabulated Relaxation Times and Fitted Parameters for **1**.[a,b,c]

	PrCN		PrCN/DMF		DMF/Tol	
T (K)	$\log_{10}(T_{1,\text{long}})$	$\log_{10}(T_{1,\text{short}})$	$\log_{10}(T_{1,\text{long}})$	$\log_{10}(T_{1,\text{short}})$	$\log_{10}(T_{1,\text{long}})$	$\log_{10}(T_{1,\text{short}})$
10	7.558(3)	6.73(1)	7.445(2)	6.66(1)	6.82(1)	6.13(1)
20	6.235(2)	5.66(1)	6.185(2)	5.67(1)	6.11(1)	5.51(1)
40	4.926(5)	4.63(2)	5.018(7)	4.75(1)	4.94(1)	4.60(1)
60	4.196(6)	3.94(1)	4.33(1)	4.06(1)	4.31(1)	4.02(1)
80	3.737(9)	3.44(1)	3.87(1)	3.56(1)	3.93(1)	3.63(1)
100	3.44(2)	3.13(1)	3.54(1)	3.21(1)	3.56(1)	3.21(1)
120	3.02(1)	2.5(3)	3.27(1)	2.96(1)	3.28(1)	2.94(2)

	d_7-DMF/d_8-Tol		CS_2	
T (K)	$\log_{10}(T_{1,\text{long}})$	$\log_{10}(T_{1,\text{short}})$	$\log_{10}(T_{1,\text{long}})$	$\log_{10}(T_{1,\text{short}})$
10	7.034(3)	6.235(6)	7.31(3)	6.50(7)
20	6.087(2)	5.472(9)	5.65(4)	6.30(2)
40	4.947(4)	4.616(9)	5.17(2)	4.63(3)
60	4.280(6)	3.96(1)	4.57(4)	4.04(4)
80	3.848(4)	3.52(1)	4.4(1)	3.79(3)
100	3.51(1)	3.16(1)	3.64(2)	3.0(2)
120	3.23(2)	2.87(3)	3.69(7)	3.1(1)

	PrCN	PrCN/DMF	DMF/Tol		*d*-DMF/Tol	CS_2	
T (K)	T_2 (μs)	T_2 (μs)	$T_{2,\text{long}}$ (μs)	$T_{2,\text{short}}$ (ns)	T_2 (μs)	$T_{2,\text{long}}$ (μs)	$T_{2,\text{short}}$ (μs)
10	1.47(1)	1.07(2)	3.25(3)	473(21)	6.5(1)	675(7)	18(1)
20	1.43(1)	1.02(1)	3.08(3)	502(20)	6.34(7)	271(3)	11(1)
40	1.34(1)	0.90(1)	2.89(3)	523(13)	6.35(2)	52.4(1)	9.4(1)
60	1.31(1)	0.798(6)	2.59(8)	635(14)	4.22(2)	16.7(5)	1.5(3)
80	1.071(2)	0.893(2)	1.006(4)	-	2.07(6)	4.6(1)	-
100	0.522(2)	0.545(1)	0.827(2)	-	1.03(1)	2.13(6)	-
120	0.108(1)	0.298(1)	0.513(2)	-	0.72(1)	1.18(4)	-
T (K)	β	β	β	β	β	β	β
10	1.21(1)	0.95(1)	-	-	0.95(2)	-	-
20	1.25(1)	0.95(1)	-	-	0.96(1)	-	-
40	1.31(1)	0.97(1)	-	-	1.23(1)	-	-
60	1.45(1)	1.15(1)	-	-	1.26(1)	-	-
80	1.26(1)	1.22(1)	1.08(1)	-	1.18(1)	-	-
100	1.23(1)	1.21(1)	1.04(1)	-	1.09(1)	-	-
120	1.00(1)	1.10(1)	1.05(1)	-	1.34(1)	-	-

[a]Solvent mixtures are 1:1 ratios. [b]Blank spaces indicate either double exponentials or stretch exponents were unnecessary to adequately fit data. [c]All $\log_{10}(T_1)$ data are computed from T_1 units in nanoseconds.

Table S7. Tabulated Relaxation Times and Fitted Parameters for **2**.[a,b,c]

	PrCN/DMF		DMF/Tol		d_7-DMF/d_8-Tol	
T (K)	$\log_{10}(T_{1,\text{long}})$	$\log_{10}(T_{1,\text{short}})$	$\log_{10}(T_{1,\text{long}})$	$\log_{10}(T_{1,\text{short}})$	$\log_{10}(T_{1,\text{long}})$	$\log_{10}(T_{1,\text{short}})$
10	7.366(3)	6.665(9)	6.852(4)	6.02(1)	6.09(1)	5.57(2)
20	6.071(5)	5.62(1)	5.88(3)	5.35(1)	5.80(1)	5.34(1)
40	4.920(3)	4.53(1)	4.883(2)	4.50(1)	4.86(1)	4.48(1)
60	4.275(3)	3.87(1)	4.270(4)	3.89(1)	4.25(1)	3.87(1)
80	3.869(3)	3.48(1)	3.803(6)	3.42(1)	3.82(1)	3.44(1)
100	3.554(7)	3.19(1)	3.47(1)	2.12(2)	3.54(1)	3.18(2)
120	3.30(1)	2.99(2)	3.16(1)	2.79(1)	3.35(1)	2.94(4)

	PrCN/DMF	DMF/Tol		d_7-DMF/d_8-Tol
T (K)	T_2 (μs)	$T_{2,\text{long}}$ (μs)	$T_{2,\text{short}}$ (μs)	T_2 (μs)
10	1.06(1)	2.87(5)	0.59(1)	6.13(7)
20	1.17(1)	2.69(5)	0.60(1)	6.26(5)
40	0.93(1)	2.43(6)	0.60(1)	5.71(2)
60	0.823(3)	0.612(4)	-	3.20(1)
80	0.850(1)	0.782(2)	-	1.96(1)
100	0.514(1)	0.673(3)	-	1.58(1)
120	0.286(2)	0.597(2)	-	0.86(1)
T (K)	β	β	β	β
10	1.03(1)	-	-	1.00(1)
20	1.16(1)	-	-	1.09(1)
40	1.09(1)	-	-	1.29(1)
60	1.25(1)	0.97(1)	-	1.27(1)
80	1.22(2)	1.23(1)	-	1.22(1)
100	1.17(1)	1.0991)	-	1.38(2)
120	0.98(1)	1.08(1)	-	1.26(1)

[a]Solvent mixtures are 1:1 ratios. [b]Blank spaces indicate either double exponentials or stretch exponents were unnecessary to adequately fit data. [c]All $\log_{10}(T_1)$ data are computed from T_1 units in nanoseconds.

Table S8. Tabulated Relaxation Times and Fitted Parameters for **3**.[a,b,c]

	PrCN/DMF		DMF/Tol		d_7-DMF/d_8-Tol	
T (K)	$\log_{10}(T_{1,\text{long}})$	$\log_{10}(T_{1,\text{short}})$	$\log_{10}(T_{1,\text{long}})$	$\log_{10}(T_{1,\text{short}})$	$\log_{10}(T_{1,\text{long}})$	$\log_{10}(T_{1,\text{short}})$
10	7.226(3)	6.565(9)	6.758(5)	6.08(1)	6.372(8)	5.769(9)
20	5.964(3)	5.554(7)	5.821(3)	5.28(1)	6.105(2)	5.513(9)
40	4.935(3)	4.582(5)	4.870(3)	4.473(6)	5.942(4)	5.60(1)
60	4.338(4)	3.929(5)	4.372(2)	3.953(3)	4.312(8)	4.02(1)
80	3.952(3)	3.514(4)	3.993(3)	3.536(4)	3.927(4)	3.620(6)
100	3.680(3)	3.234(5)	3.723(3)	3.276(5)	3.556(7)	3.210(9)
120	3.425(5)	3.006(8)	3.486(8)	3.06(1)	3.279(8)	2.94(2)

	PrCN/DMF	DMF/Tol		d_7-DMF/d_8-Tol
T (K)	T_2 (μs)	$T_{2,\text{long}}$ (μs)	$T_{2,\text{short}}$ (μs)	T_2 (μs)
10	1.08(1)	2.59(3)	0.54(1)	6.01(1)
20	1.04(1)	2.56(3)	0.55(1)	5.77(4)
40	0.95(1)	2.29(2)	0.56(1)	5.64(2)
60	0.85(3)	0.67(1)	-	3.66(2)
80	0.88(1)	0.796(3)	-	2.30(4)
100	0.573(1)	0.708(3)	-	1.38(5)
120	0.334(3)	0.575(2)	-	0.765(6)
T (K)	β	β	β	β
10	1.06(1)	-	-	0.99(2)
20	1.07(1)	-	-	1.11(1)
40	1.12(1)	-	-	1.28(1)
60	1.24(1)	0.95(1)	-	1.31(1)
80	1.230(2)	1.07(1)	-	1.24(1)
100	1.183(2)	0.99(1)	-	1.11(4)
120	0.98(1)	1.00(3)	-	1.03(6)

[a]Solvent mixtures are 1:1 ratios. [b]Blank spaces indicate either double exponentials or stretch exponents were unnecessary to adequately fit data. [c]All $\log_{10}(T_1)$ data are computed from T_1 units in nanoseconds.

Table S9. Tabulated Relaxation Times and Fitted Parameters for **4**.[a,b,c]

	PrCN/DMF		DMF/Tol		d_7-DMF/d_8-Tol	
T (K)	$\log_{10}(T_{1,\text{long}})$	$\log_{10}(T_{1,\text{short}})$	$\log_{10}(T_{1,\text{long}})$	$\log_{10}(T_{1,\text{short}})$	$\log_{10}(T_{1,\text{long}})$	$\log_{10}(T_{1,\text{short}})$
10	7.244(3)	6.53(1)	7.021(4)	6.167(9)	6.025(5)	5.44(1)
20	5.893(4)	5.49(1)	5.887(3)	5.351(9)	5.770(4)	5.21(1)
40	4.551(5)	4.889(4)	4.881(4)	4.489(8)	4.845(5)	4.44(1)
60	4.284(3)	3.916(5)	4.301(5)	3.912(6)	4.295(3)	3.891(4)
80	3.928(5)	3.545(7)	3.945(3)	3.540(4)	4.007(4)	3.596(4)
100	3.633(5)	3.259(6)	3.701(6)	3.299(7)	3.68(1)	3.269(9)
120	3.394(8)	3.029(8)	3.40(1)	3.02(1)	3.50(2)	3.09(2)

	PrCN/DMF	DMF/Tol		d_7-DMF/d_8-Tol
T (K)	T_2 (μs)	$T_{2,\text{long}}$ (μs)	$T_{2,\text{short}}$ (μs)	T_2 (ns)
10	1.024(9)	2.79(4)	0.57(1)	6.33(9)
20	1.000(7)	3.3(1)	0.62(1)	5.79(6)
40	0.896(6)	2.8(1)	0.593(9)	5.642(8)
60	0.854(4)	0.679(8)	-	3.507(5)
80	0.837(1)	0.781(3)	-	2.314(4)
100	0.555(1)	0.705(2)	-	1.52(2)
120	0.308(1)	0.643(2)	-	0.96(5)
T (K)	β	β	β	β
10	1.02(2)	-	-	1.06(2)
20	1.03(1)	-	-	1.04(1)
40	1.08(1)	-	-	1.274(2)
60	1.25(1)	1.04(1)	-	1.26(3)
80	1.21(1)	1.12(1)	-	1.25(1)
100	1.18(1)	1.02(1)	-	1.24(2)
120	1.10(1)	1.01(1)	-	1.24(6)

[a]Solvent mixtures are 1:1 ratios. [b]Blank spaces indicate either double exponentials or stretch exponents were unnecessary to adequately fit data. [c]All $\log_{10}(T_1)$ data are computed from T_1 units in nanoseconds.

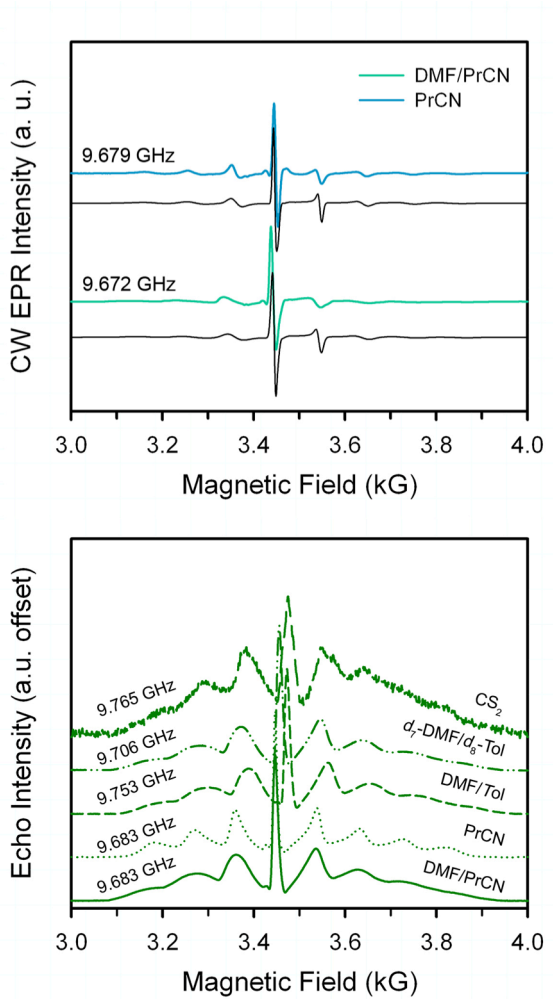

Figure S1 | Variable-solvent continuous wave (top) and echo-detected (bottom) X-band EPR spectra for 1 and 1′ at 40 K. Data were collected on 0.5 mM frozen solutions except for CS_2, which was 0.01 mM in analyte. Specific frequencies for each measurement are given in the figure. The employed two-pulse Hahn echo sequence used $^{\pi}/_{2}$ and π pulse lengths of 32 and 48 ns, respectively, with 140 ns inter-pulse delay time for all spectra; CS_2 data were collected with a 160 ns inter-pulse delay time. Simulations of the cw spectra employed g and $\boldsymbol{A}$ values listed in Table S5.

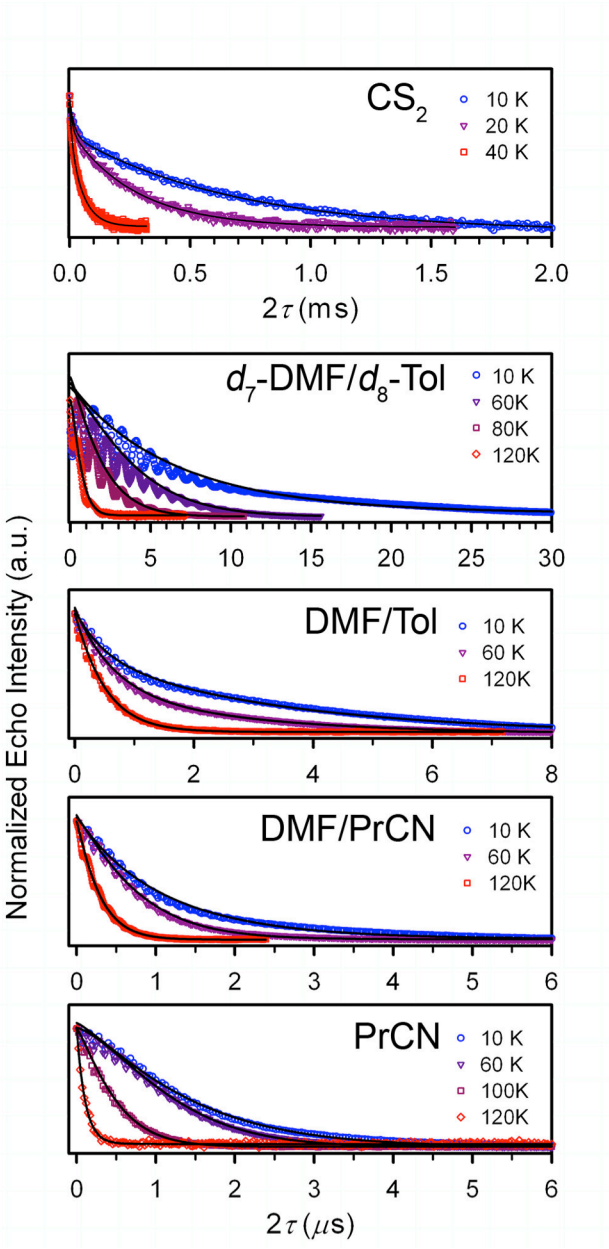

Figure S2 | Select variable-temperature echo decay curves for 1 and 1′ in various solvents. The employed two-pulse Hahn echo sequence used $^{\pi}/_{2}$ and π pulse lengths of 32 and 48 ns, respectively. Note the timescale difference between the CS_2 data versus the other solvent systems. Black lines represent best fits to exponential decays, yielding T_2 values depicted in Fig. 2 in the main text (see spectroscopy experimental section for details).

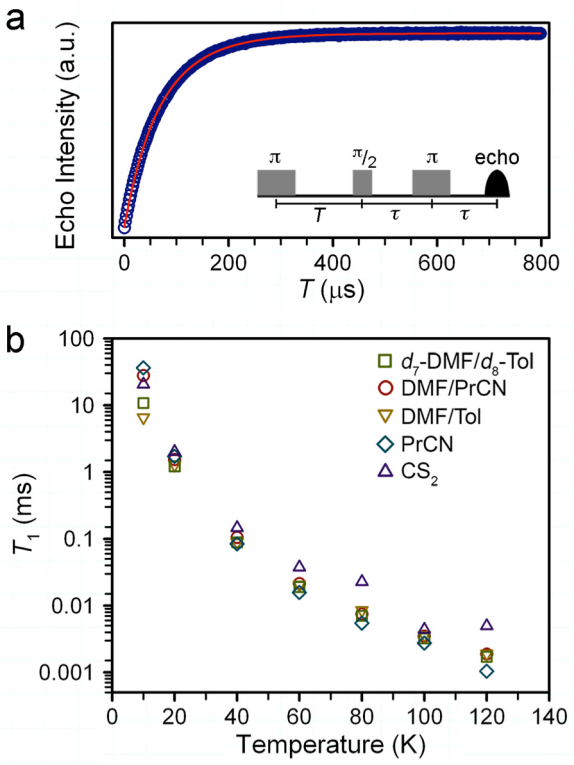

Figure S3 | Variable-temperature inversion recovery data for 1 and 1′ in various solvents. **a.** Inversion recovery curve for 0.5 mM solution of **1** in PrCN at 40 K and H_{dc} = 3445 Oe. The red line is a best fit to a biexponential function with T_1 = 84.3(1) μs. The inversion recovery pulse sequence is depicted. **b.** Temperature dependence of the T_1 data in the given solvents. Errors in T_1 values are within the symbol size.

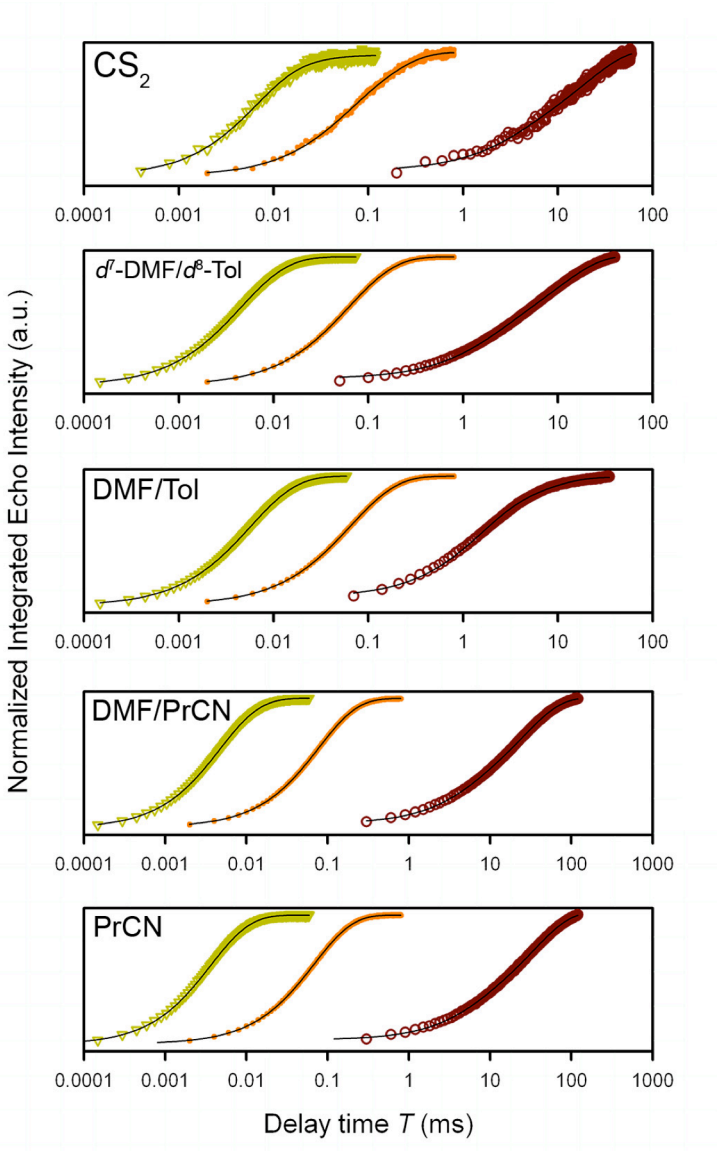

Figure S4 | Select variable-temperature inversion recovery curves for 1 and 1′ in various solvents. The employed two-pulse Hahn echo sequence used $^{\pi}/_{2}$ and π pulse lengths of 32 and 48 ns, respectively, for all solvents except CS_2. For CS_2, pulse lengths of 28 and 44 ns were used. Note the timescales are the same for all data. Black lines represent best fits to biexponential recoveries (see spectroscopy experimental section for details).

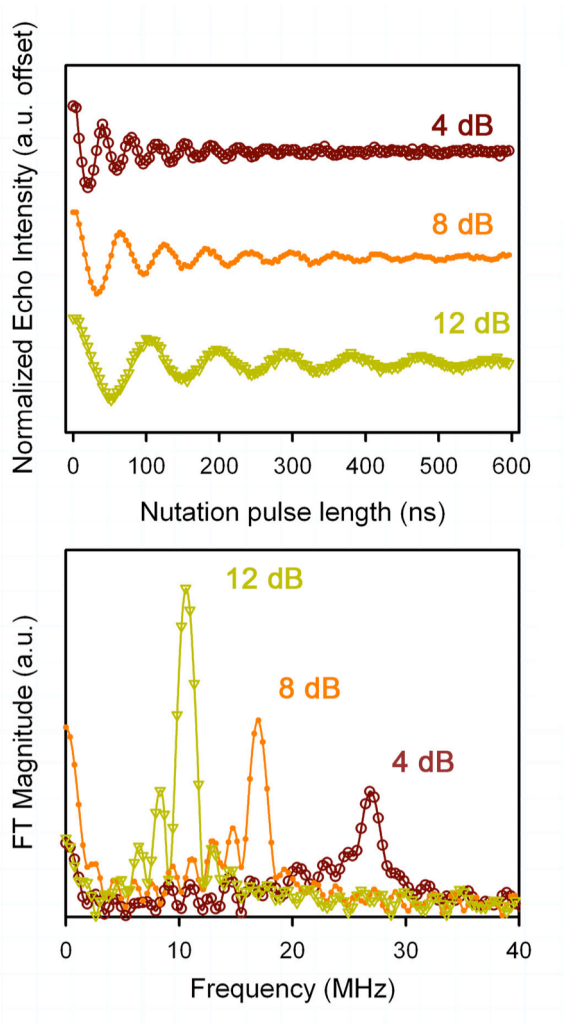

Figure S5 | Variable B_1 nutations for 1′ (top) and corresponding Fourier transforms (bottom). Fourier transforms were performed with data zero filled with 1024 points and a Hamming window. Peak maxima in the bottom figure correspond to 10.57, 16.99, and 26.81 MHz for 12, 8, and 4 dB attenuation levels of the mw power, respectively. π operation times were determined from these maxima and are give in the inset to Figure 3 in the main text. Solid lines are guides for the eye.

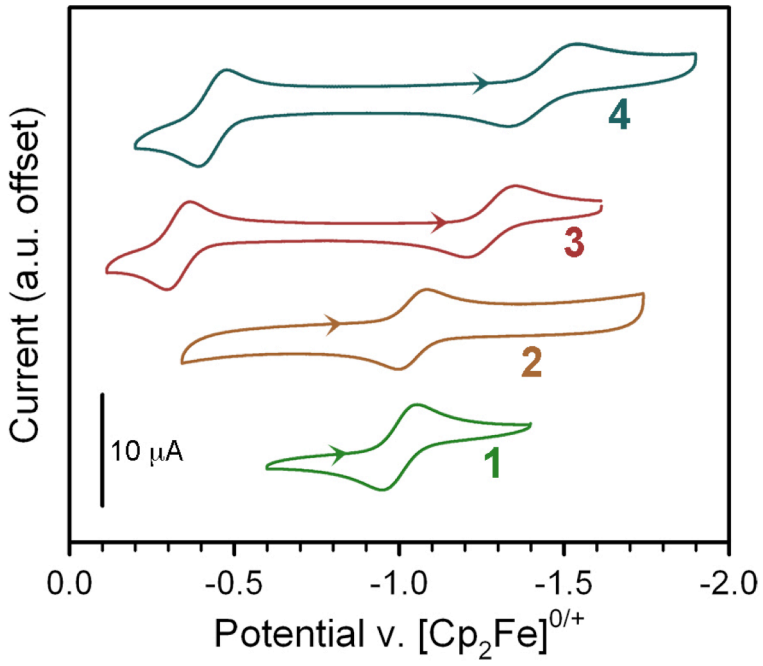

Figure S6 | Cyclic voltammetry data for 1-4. Data were collected at room temperature in MeCN solutions with 0.1 mM $(Bu_4N)PF_6$ supporting electrolyte and a platinum electrode. Scans proceeded at 600 mV/s in the directions indicated by the arrows on each data set. Reductive waves of $E_{1/2}$ = –1.002, –1.039, –1.275, and –1.467 V vs. $Cp_2Fe^{0/+}$, respectively, are observed for **1-4**. Compounds **3** and **4** display additional waves at more positive potentials: –0.329 and –0.465 mV vs. $Cp_2Fe^{0/+}$, respectively. Comparison of these results to electrochemical analyses of other vanadium dithiolate complexes suggests the reductive waves are metal-centered redox events, while the oxidative waves involve the ligands.[18] Rest potentials are slightly more positive than the observed waves of **1** and **2** and the reductive waves in **3** and **4**.

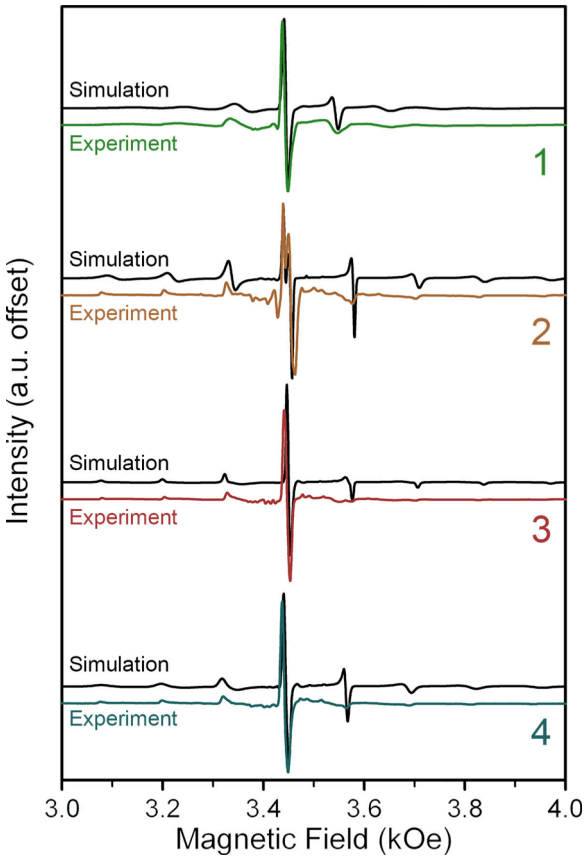

Figure S7 | Continuous-wave X-band (9.67-9.68 GHz) EPR spectra for 1-4. Spectra were collected on frozen solutions at 0.5 mM concentration in 1:1 DMF/PrCN. Cw-spectra were acquired at 100 K. Colored lines represent experimental data and the black lines are the best simulations affording the parameters in Table 1. Data for **1** are the same as those in Figure S1 but are depicted here for ease of comparison. Parameters for each simulated spectrum are given in Table S5.

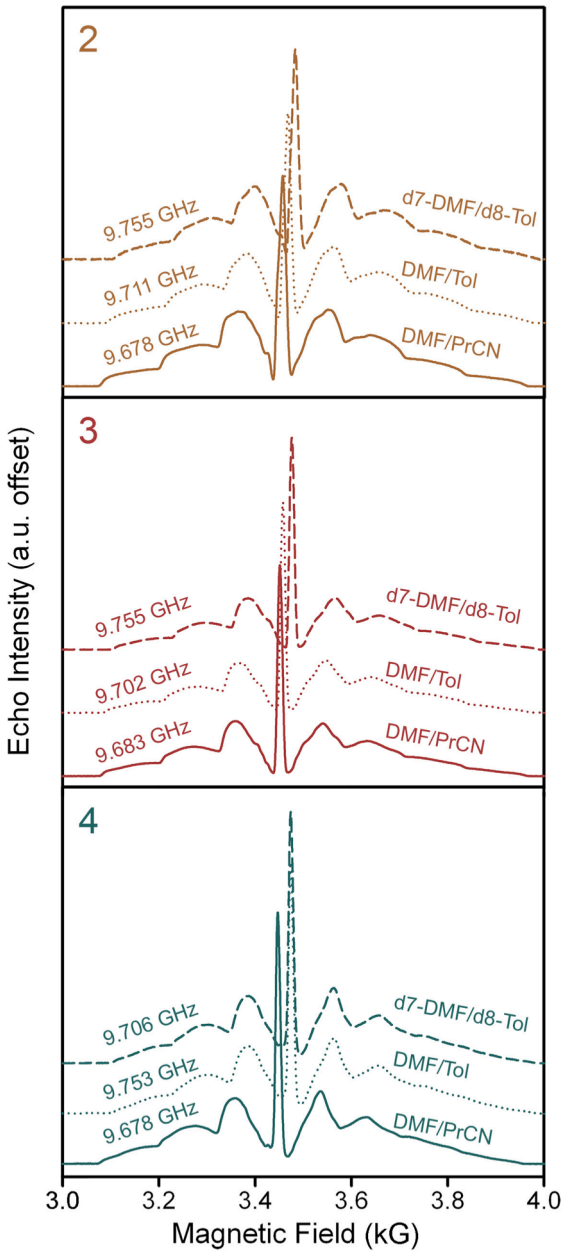

Figure S8 | Variable-solvent echo-detected field-swept X-band EPR spectra for 2-4. Data were collected on frozen solutions (0.5 mM in analyte) at 40 K. Specific frequencies for each measurement are provided in the Figure. The employed two-pulse Hahn echo sequence used $^{\pi}/_{2}$ and π pulse lengths of 32 and 48 ns, respectively, with 140 ns inter-pulse delay time for all spectra.

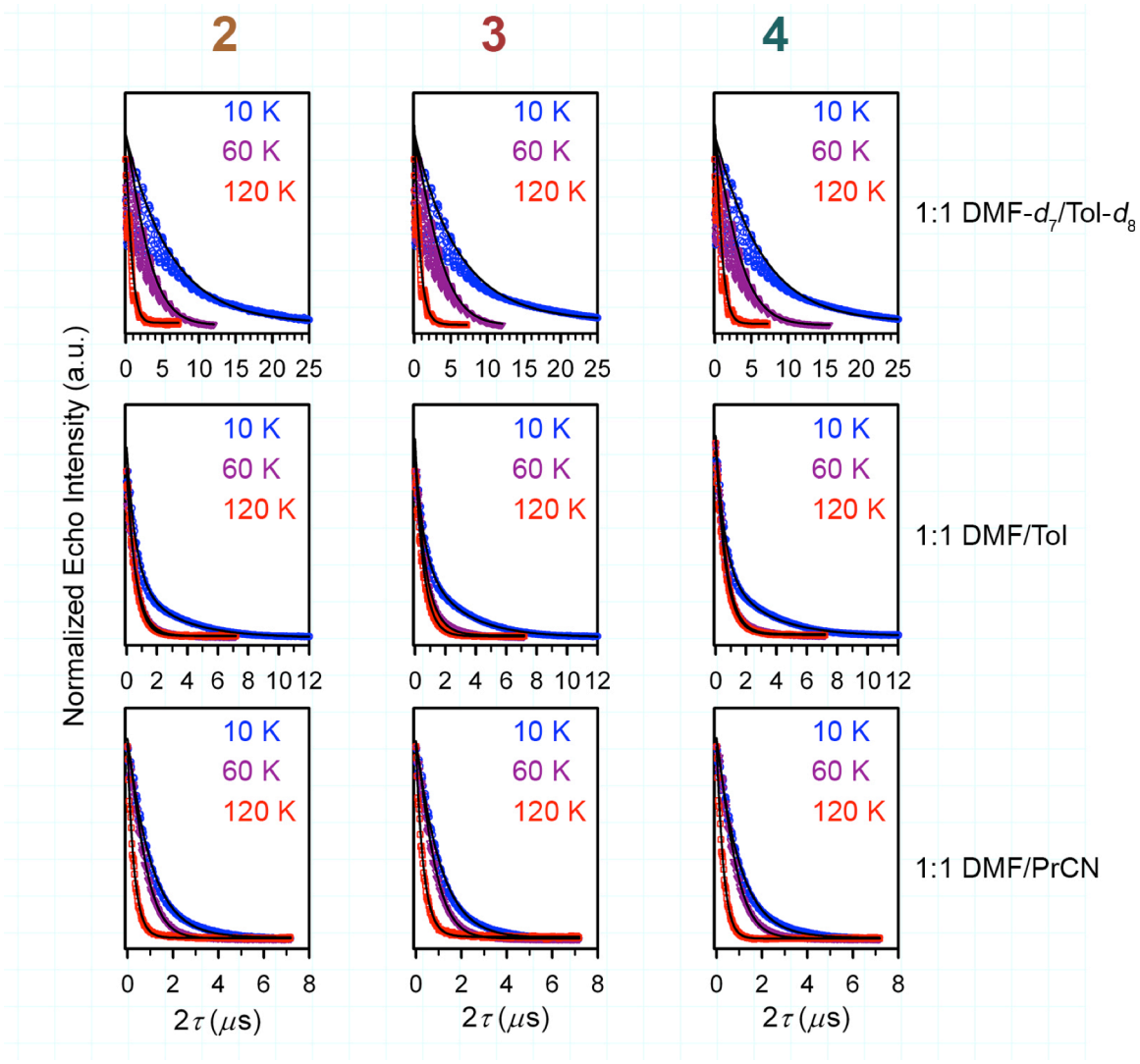

Figure S9 | Select variable-temperature, variable-solvent Hahn echo decay curves 2-4. Black lines are the best fits of the data to exponential decays. T_2 values obtained at these temperatures are graphically depicted in Figure S6. Selected temperatures as opposed to the entire data set are depicted for clarity. Data were collected at the peak of maximum echo intensity in Fig. S5.

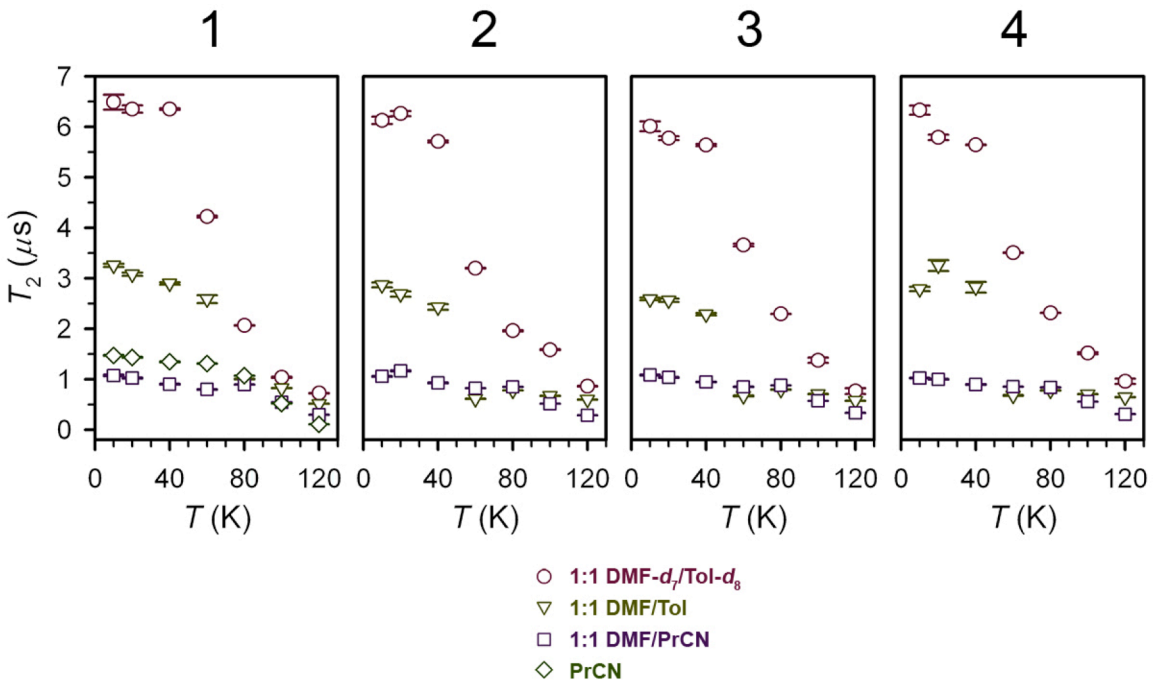

Figure S10 | T_2 values for 1-4 as a function of solvent and temperature. T_2 values were determined by fitting variable echo decay curves to exponentially decaying functions. Error bars are depicted; note for most temperature points error bars are smaller than the symbols.

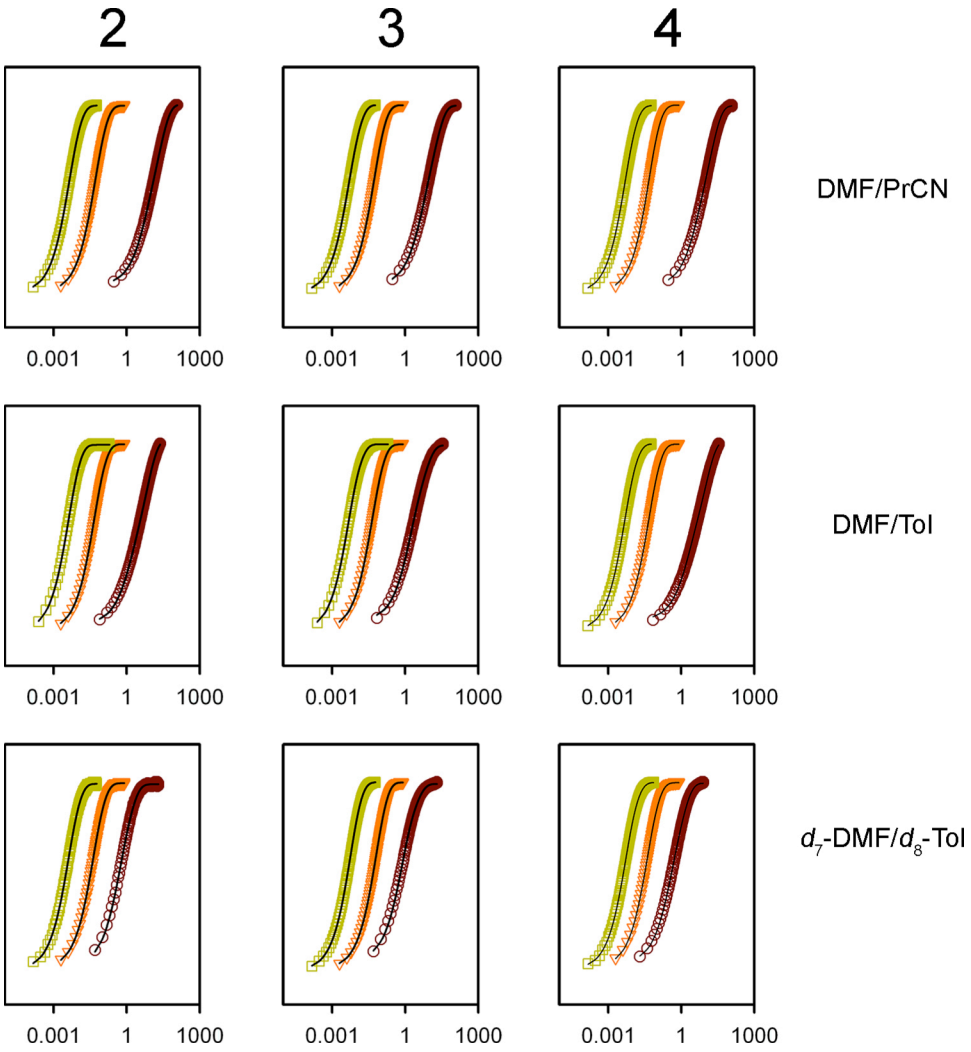

Figure S11 | Select inversion recovery curves for 2-4 in three different solvent systems. Temperatures are 10 K (yellow), 40 K (orange) and 80 K (red). Black lines represent best fits to biexponential fits with the T_1 values depicted in Figures S10 and S11. All data were collected at the sharpest resonances in the edfs spectra (Fig. S5).

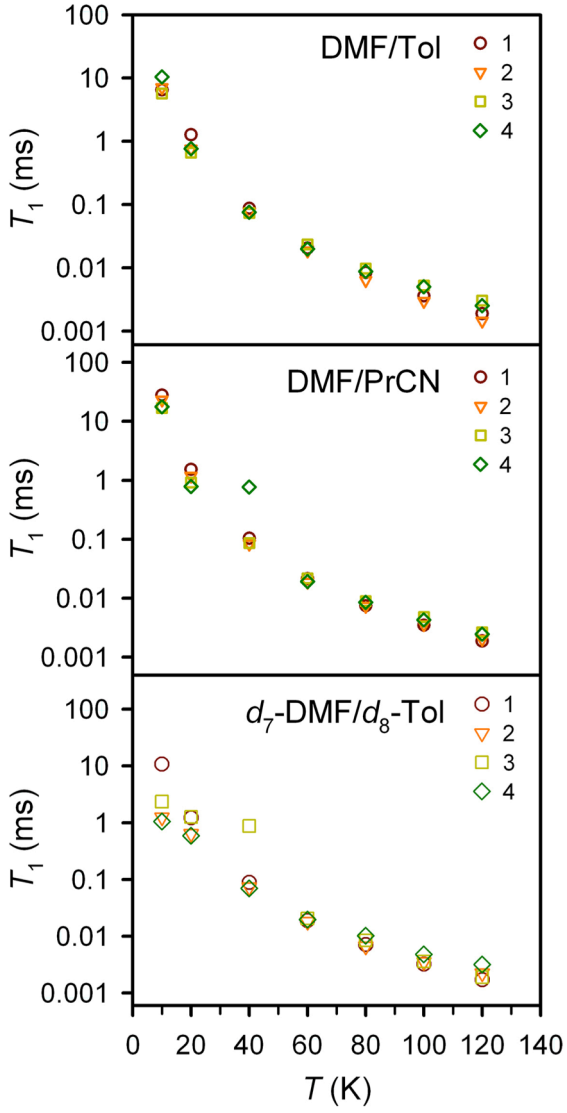

Figure S12 | Variable temperature T_1 data for 1-4 organized by solvent system. Each panel shows the temperature dependence of T_1 for all four complexes in the solvent system given in the panel. All data were collected on 0.5 mM solutions for each solvent combination and result from inversion recovery experiments (Figs. S3 and S9).

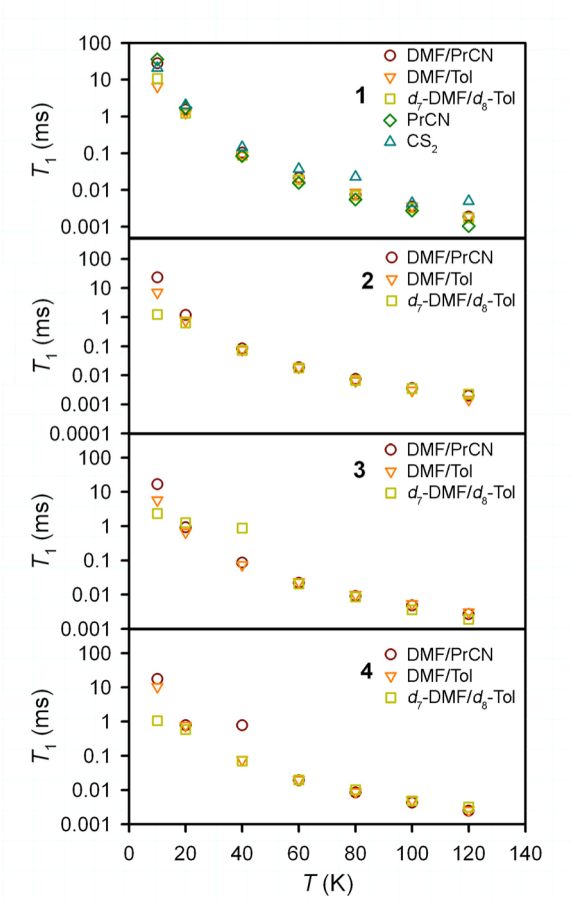

Figure S13 | Variable-temperature T_1 for 1-4 organized by molecule. Each panel depicts the temperature dependence of a single compound in the specified solvents. Numbers in each panel signify the compound being measured. Data were extracted by inversion recovery measurements (Figs. S3 and S10).

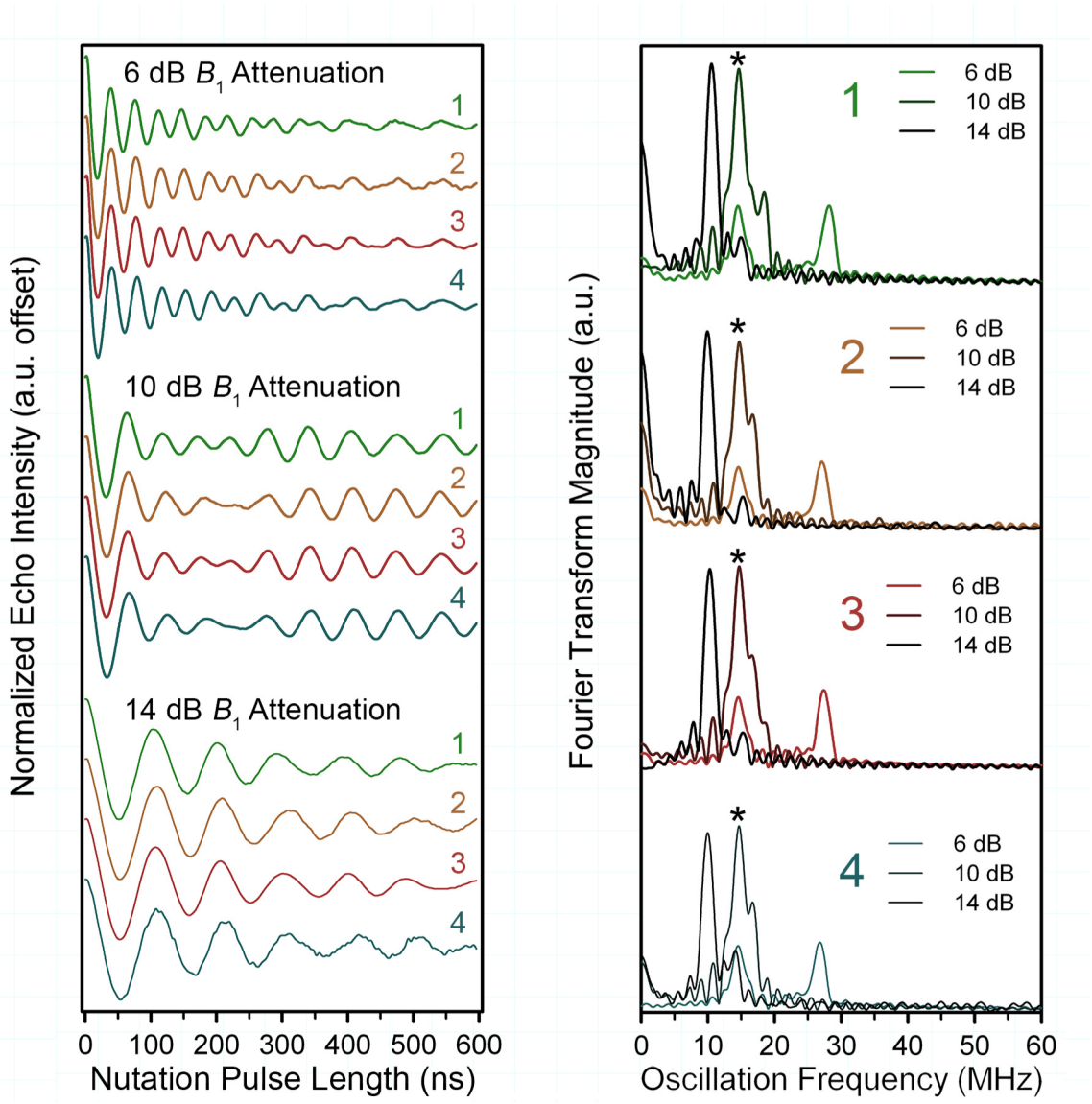

Figure S14 | Variable-B_1 nutation data (left) and Fourier Transforms of the data for 1-4 (right) in DMF/PrCN. The asterisks in the plots of the Fourier transform magnitude indicate peaks at 14.7 MHz. This value is extremely close to the Larmor frequency of ^{1}H (14.69 MHz) at the fields of measurement (3450±5 Oe, for **1-4** respectively). The appearance of such a peak when the frequency of the Rabi oscillation approaches the Larmor frequency of a nucleus arises from the Hartman-Hahn effect.[13]

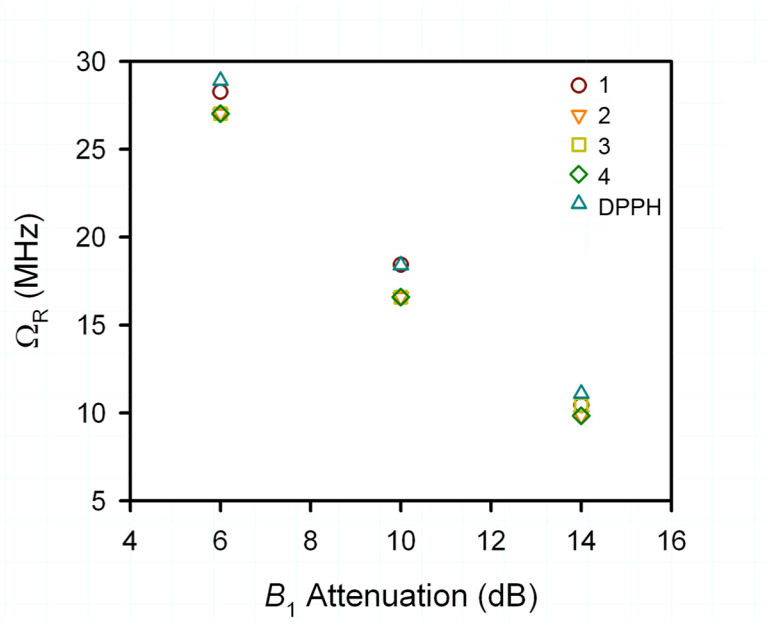

Figure S15 | Rabi frequencies as a function of B_1 attenuation for 1-4. Data were determined by the peak locations in the Fourier transforms of the nutation data. Nutation frequencies from an $S = {}^1/_2$ standard, 2,2-diphenyl-1-picrylhydrazyl radical (DPPH), are also provided.

References

1. Hansen, T. K.; Becher, J.; Jørgensen, T.; Varma, K. S.; Khedekar, R.; Cava, M. P. 4,5-Dibenzoyl-1,3-dithiole-1-thione (benzenecabothioic acid, S, S'-(2-thioxo-1,3-dithiole-4,5-diyl) ester). *Org. Synth.* **1998***, 73,* 270.
2. Steimecke, G.; Sieler, H.; Kirmse, R.; Dietzsch, W.; Hoyer, E. 1,2-Dithiol-3-thione-4,5-dithiolate from carbon disulfide and alkali metal. *Phosphorus Sulfur* **1982**, *12*, 237.
3. Manzer, L. E. Tetrahydrofuran complexes of selected early transition metals. *Inorg. Synth.* **1982**, *21*, 135.
4. Prepared following the prep of Marcoux and Charette starting with C_6D_5Br and $P(C_6D_5)_3$. Marcoux, D.; Charette, A. B. Palladium-catalyzed synthesis of functionalized tetraarylphosphonium salts. *J. Org. Chem.* **2008**, *73*, 590.
5. Schumaker, R. R.; Lee, V. Y.; Engler, E. M. Noncoupling synthesis of tetrathiafulvalenes. *J. Org. Chem.* **1984**, *49*, 564.
6. Okubo, T.; Maeda, R.; Kondo, M.; Mitani, T.; Kitagawa, S. A new honeycomb assemblage of a trisdithiolene vanadium(IV) complex, $(PPh_4)_2[V(dbddto)_3](C_6H_4Cl_2)(hexane)_{0.5}$. *Chem. Lett.* **2006**, *35*, 34-35.
7. Armarego, W. L. F.; Chai, C. L. L. *Purification of Laboratory Chemicals*, 7th ed.; Oxford: Butterworth-Heinemann, 2012.
8. *APEX2*, v. 2009 ; Bruker Analytical X-Ray Systems, Inc: Madison, WI, 2009.
9. Sheldrick, G. M. *SADABS*, Version 2.03; Bruker Analytical X-Ray Systems, Inc.: Madison, WI, 2000.
10. Sheldrick, G. M. *SHELXTL*, Version 6.12; Bruker Analytical X-ray Systems, Inc.: Madison, WI, 2000
11. Dolomanov, O. V.; Bourhis, L. J.; Gildea, R. J.; Howard, J. A. K.; Puschmann, H. OLEX2: a complete structure solution, refinement and analysis program. *J. Appl. Cryst.* **2009**, *42*, 339-341.
12. Origin; OriginLab, Northampton, MA, United States.
13. Hartmann, S. R.; Hahn, E. L. Nuclear double resonance in the rotating frame. *Phys. Rev.* **1962**, *128*, 2042.
14. Stoll, S.; Schweiger, A. EasySpin, a comprehensive software package for spectral simulation and analysis in EPR. *J. Magn. Reson.* **2006**, *178*, 42.
15. Diamantis, A. A.; Raynor, J. B.; Rieger, P. H. *J. Chem. Soc., Dalton Trans.* **1980**, 1730.
16. Branca, M.; Micera, G.; Dessi, A.; Sanna, D.; Raymond, K. N. Re-examination of the electron spin resonance spectrum of trigonal-prismatic bis[pentane-2,4-dionebenzoylhydrazonato(2-)] vanadium(IV). *Inorg. Chem.* **1990,** *29*, 1586-1589.
17. Spikes, G. H.; Sproules, S.; Bill, E.; Weyhermüller, T.; Wieghardt, K. One- and two-electron reduced 1,2-diketone ligands in $[Cr^{III}(L^{\bullet})_3]$ ($S = 0$) and $Na_2(Et_2O)_2[V^{IV}(L^{Red})_3]$ ($S = {}^1/_2$). *Inorg. Chem.* **2008**, *47*, 10935-10944.
18. Sproules, S.; Weyhermüller, T.; DeBeer, S.; Wieghardt, K. *Inorg. Chem.* Six-membered electron transfer series $[V(dithiolene)_3]^z$ (z = 1+, 0, 1–, 2–, 3–, 4–). An X-ray Absorption Spectroscopic and Density Functional Theoretical Study. **2010**, *49*, 5241-5261.